Non-Debye to Debye transition of ac dielectric response in $YCrO_3$ nanoceramic under sintering: effect of pore structure

2008 J. Phys.: Condens. Matter 20 345201

(http://iopscience.iop.org/0953-8984/20/34/345201)

J. Phys.: Condens. Matter **20** (2008) 345201 (7pp) doi:10.1088/0953-8984/20/34/345201

Non-Debye to Debye transition of ac dielectric response in $YCrO_3$ nanoceramic under sintering: effect of pore structure

J Bahadur[1], D Sen[1], S Mazumder[1,3], R Shukla[2] and A K Tyagi[2]

[1] Solid State Physics Division, Bhabha Atomic Research Centre, Mumbai, India
[2] Chemistry Division, Bhabha Atomic Research Centre, Mumbai, India

E-mail: smazu@barc.gov.in

Received 25 March 2008, in final form 15 July 2008
Published 1 August 2008
Online at stacks.iop.org/JPhysCM/20/345201

Abstract

Dielectric response of the porous $YCrO_3$ nanoceramic has been investigated as a function of sintering temperature. Pore structure at different sintering temperatures has been studied by small-angle neutron scattering (SANS). It has been observed that overall polydispersity of pore-size distribution decreases and loss peak of the ac dielectric response gets pronounced with a slight peak shift towards higher frequency with increasing sintering temperature. A non-Debye to Debye type transition of the dielectric response is observed beyond a sintering temperature of 1400 °C. Dielectric results were explained on the basis of pore morphology, pore-size distribution and connectivity between the pores.

(Some figures in this article are in colour only in the electronic version)

1. Introduction

Dielectric properties of heterogeneous materials, in particular porous materials, have been the subject of immense interest for quite some time [1]. This is partially due to a need for understanding the electrical properties of various technological materials and also to understand the fundamental physics aspect of the charge carrier transport phenomenon in heterogeneous materials. Propagation of electromagnetic waves in disordered materials leads to an interesting question about the theoretical description of physical phenomena like many-body interactions (dipole–dipole, ion–ion or electron–electron interactions) in such materials [2]. In particular, biferroic materials, which possess both ferromagnetic and ferroelectric properties, are of special interest because of their potential technological applications [3]. Recently $YCrO_3$, a rare-earth chromate, has been observed as biferroic in nature [4]. In general, dielectric properties of materials may be represented by a complex electrical permittivity $\varepsilon^* = \varepsilon' + i\varepsilon''$. The complex part of the permittivity (ε'') is a measure of energy dissipation in the material. Dielectric loss is generally described in terms of the loss tangent, $\tan(\delta) = \frac{\varepsilon''}{\varepsilon'}$. The various polarization mechanisms manifest in different frequency regions of dielectric spectra and the value of the relative permittivity is governed by different polarization mechanisms in different frequency regimes. In general, the dielectric response in materials is of two kinds. In the first kind, the dielectric response arises due to charge carriers and usually appears at a relatively lower frequency regime of the dielectric spectra. This is also called anomalous low frequency dispersion (ALFD) and was identified by Jonscher for the first time [5]. The second kind of universal response involves a relaxation process. This occurs primarily in dipolar systems. But in some cases low mobility charge carriers are also responsible for this type of behavior [6]. Factors which affect the dielectric constant and loss are broadly classified into two categories: intrinsic and extrinsic. Intrinsic losses are dependent on the crystal structure and can be described in terms of the interaction of the phonon system with the alternating electric field, whereas extrinsic losses depend on the heterogeneity of the medium such as porosity, impurities, grain boundaries, micro-cracks, random crystal orientation, etc [7–9]. Electrically heterogeneous materials may experience interfacial polarization. In these materials, the motion of charge carriers may occur easily through one phase and therefore the motion of charge carriers is constricted at phase

[3] Author to whom any correspondence should be addressed.

Table 1. Important parameters from SANS and dielectric measurements.

Sintering temperature (°C)	Porosity (%)	Actual density (%TD)	$\langle R\rangle$ (nm)	$[\langle R^2\rangle - \langle R\rangle^2]^{0..5}$ (nm)	f_p (Hz)	m	n	$(1-n)$
1300	61	39	14.3	16.9	1.6×10^3	0.42	0.25	−0.75
1400	59	41	8.5	9.1	0.8×10^3	0.39	0.28	−0.72
1500	42	58	8.8	7.9	5.6×10^4	1.0	0.005	−2
1600	22	78	7.6	6.5	4.0×10^4	0.99	0	−2

boundaries. For example, in porous materials pores can be considered as inhomogeneities in a solid matrix. Charge carrier movement through the solid matrix is relatively easier as compared to movements through pores. As a result, charge builds up at interfaces and forms a dipole. These dipoles can be polarized in the external applied electric field. Such effects are known as Maxwell–Wagner effects [10, 11]. Thus, interfacial polarization plays a significant role in porous materials as far as its dielectric response is concerned.

Sintering is a thermal treatment that binds particles together into a solid coherent structure by means of mass transport mechanisms occurring largely at the atomic level. The initial powder (called a green powder) has a large surface area relative to its volume. This surface area provides the driving force in sintering, which is the reduction of the free surface energy resulting from the high surface area of the particles. Thus, sintering controls the microstructure in a mesoscopic length scale. In this way, sintering controls pore morphology and porosity in materials [12].

Small-angle neutron scattering (SANS) is an important and non-destructive technique to probe the mesoscopic structure in ceramics and other porous materials [13–17]. SANS has an advantage for investigating pore structure in ceramics compared to other techniques such as BET, mercury porosimetry, etc, as SANS can probe open as well as closed porosity in the specimen.

The present work deals with SANS investigation on pore characteristics and the effect of pore structure on the low and intermediate frequency (0.02–1000 kHz) dielectric response of $YCrO_3$ nanoceramic at different sintering temperatures.

2. Experimental details

2.1. Sample preparation

Nanocrystalline $YCrO_3$ has been prepared by a gel-combustion technique. Details of the preparation method have been described elsewhere [18]. For the present study, the powder has been calcined at 600 °C to obtain a chemically pure and crystalline product. The initial powder characterization has been described in an earlier paper [18]. The resulting nanocrystalline powder was cold pressed into pellets at a compaction pressure of 200 MPa using a hydraulic press.

The pellets were sintered at temperatures of 1300, 1400, 1500 and 1600 °C. The porosity measurements have been carried out by the gravimetric method. The measured porosity values are tabulated in table 1.

2.2. SANS

SANS experiments have been performed using a double-crystal-based medium resolution small-angle neutron scattering instrument (MSANS) at the Guide Tube Laboratory of the Dhruva rector at Trombay, India [19a]. The instrument consists of a non-dispersive $(1, -1)$ setting of (111) reflections from silicon single crystals with the specimen between two crystals. The scattered intensities have been recorded as a function of wavevector transfer q $(= 4\pi \sin(\theta)/\lambda$, where 2θ is the scattering angle and λ $(= 0.312$ nm) is the incident neutron wavelength for the present experiment). Measurements have been performed on pellets which were sintered at temperatures of 1300, 1400, 1500 and 1600 °C. To access a higher q range, experiments have also been performed using a 5 m long slit-geometry SANS diffractometer at the Guide Tube Lab at Dhruva, India [19b]. It makes use of a BeO filter as a monochromator. The beam passes through two slits S_1 and S_2 before it is incident on the sample. The angular distribution of neutrons scattered by the sample is recorded using a 1 m long linear position-sensitive detector. SANS profiles were recorded in the q range 0.003–0.17 nm^{-1} by MSANS and in the q range 0.17–3.5 nm^{-1} by slit-based SANS. In order to correct the multiple scattering effects for the above specimens, SANS experiments were performed for two different thicknesses of each specimen in order to correct the multiple scattering effect [20]. SANS profiles of the specimens were corrected for the smearing effect using the method given in the literature [21] prior to further analysis.

2.3. Dielectric measurements

Capacitance and $\tan(\delta)$ values have been measured using a RLC bridge in the frequency range 0.2–100 kHz. Values of the relative permittivity (ε_r') at various frequencies have been calculated from the measured capacitance values by using the appropriate geometric factor. The imaginary part (ε_r'') has been calculated by multiplying ε_r' with $\tan(\delta)$. The real and imaginary parts of the electrical permittivity are shown in figures 5 and 6, respectively.

3. Data analysis and discussion

In traditional small-angle scattering (SAS) experiments using 'thin samples', scattering data are interpretable in terms of laws based on the single-scattering approximation. In such cases the functionality or shape of the scattering profile is invariant with respect to sample thickness or wavelength of the probing radiation. In other words, the scattering profiles recorded with

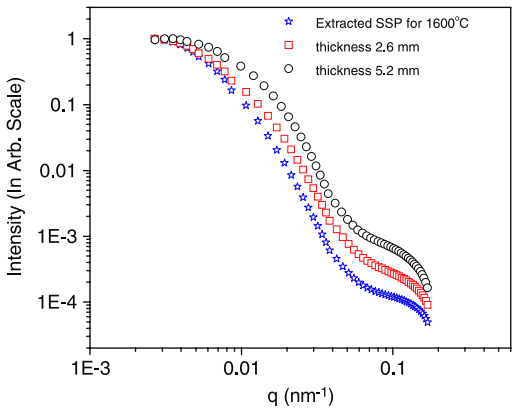

Figure 1. SANS profiles (from MSANS) for 1600 °C sintered pellets for two thicknesses are shown. The corresponding extracted single-scattering profile is compared with the experimental profiles for two thicknesses.

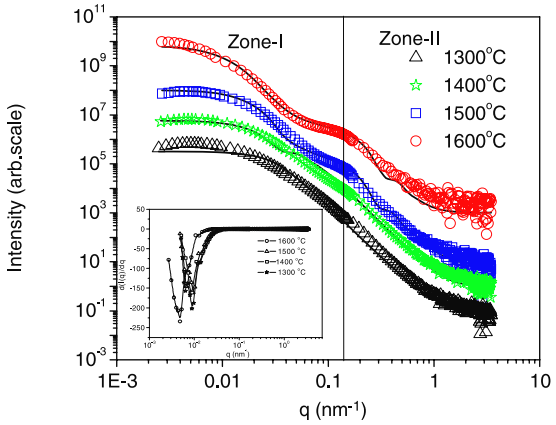

Figure 2. Multiple-scattering corrected SANS profiles with model fit for different sintering temperatures. The inset of the figure shows the derivative of the intensity with q.

variation of sample thickness or wavelength are different as regards a scale factor only. They become indistinguishable from each other after suitable normalization or when the absolute intensities are used to represent the scattering profiles.

SAS data from porous systems are often affected by multiple scattering [21]. The influence of multiple scattering in SAS data arises due to one or more of these factors: strong contrast, long wavelength, large inhomogeneities and significant thickness of the sample. Very often, factors like strong contrast, long wavelength and large inhomogeneities reduce the scattering mean free path (SMFP) l to such an extent that there is a gross violation of the single-scattering approximation which demands that thickness should be infinitesimally small in comparison to the SMFP. But often samples supposed to replicate the bulk matrix in essential properties are too thick for the single-scattering approximation to be valid.

The signature of multiple scattering is the functional dependence of measured profiles on the sample thickness or the wavelength of the probing radiation [22, 23a].

A measure of multiple scattering is generally quantified by scattering power (N), which is the ratio of sample thickness

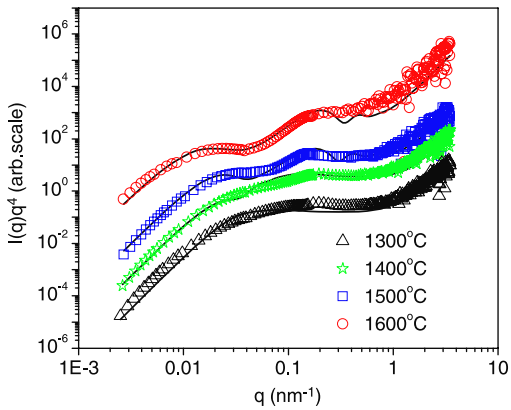

Figure 3. SANS profiles for different sintering temperatures with the model fit in Porod representations.

(t) to the mean free path (l) of the neutrons [22, 23a]. The single-scattering profile can be extracted from the recorded profiles for two different thicknesses of the specimens or for two different wavelengths of the neutron [22].

The algorithm for inversion of multiple-scattering profile into single-scattering profile (SSP) is based on the principle that, although the different multiple-scattering profiles are functionally distinct with N, the computed SSP from each of them is functionally the same or at least deviated, provided the correct N value is used for the inversion [22]. The most important step of this algorithm [22] is the estimation of N for each measurement from the two computed $g_j(r)$ $(j = 1, 2)$ functions in real space obtained by the Hankel transformation $[g(r) = \int q I(q) J_0(qr)\, \mathrm{d}q]$ of two SANS profiles $I_j(q)$.

To determine scattering mean free path (l) from measurements with two different thicknesses, the following function: $\sum_i [Y_1(r_i, \frac{t_1}{l}) - Y_2(r_i, \frac{t_2}{l})]^2$, is minimized with respect to l. The function $Y(r, N) = \frac{1}{N} \ln[\frac{g(r)}{g(0)}[\mathrm{e}^N - 1] + 1]$ is proportional to the Hankel transform of the SSP.

SANS profiles for two different thicknesses corresponding to a specimen sintered at 1600 °C are depicted in figure 1. The profiles are normalized at the lowest accessible q value in order to compare the functionality of the two profiles. It is evident from the figure that the profiles are significantly modified with variation in the sample thickness and hence the effect of multiple scattering in the present case cannot be neglected. Using the methodology as described above, the corresponding SSP, extracted from the multiple-scattering profiles (for two different thicknesses) is depicted in figure 1. It is evident that the extracted SSP is sharper as compared to the recorded profiles which are affected by multiple scattering. Similarly, for other recorded profiles, the SSP was extracted with the above-mentioned algorithm.

The corrected SANS profiles are plotted in figure 2 for different sintering temperatures. SANS profiles are also depicted in the Porod plot ($I(q)q^4$ versus q) in figure 3.

It is evident from table 1 that the porosity decreases with increasing sintering temperature. It is observed from figures 2 and 3 that SANS profiles get significantly modified as sintering temperature is increased.

A shoulder-like feature (at $q \sim 0.15$ nm^{-1}) starts appearing at 1400 °C and becomes more pronounced at higher sintering temperatures. But the observed shoulder position does not shift appreciably with sintering temperature.

To explain these features of the scattering data a model as described below has been adopted The intensity from an ensemble of mono-disperse pores in a matrix is given by

$$I(q) \propto \frac{\mathrm{d}\Sigma(\Omega)}{\mathrm{d}\Omega} = \tau(\rho_{\mathrm{matrix}} - \rho_{\mathrm{pores}})^2 V_{\mathrm{p}}^2 P(q) \qquad (1)$$

where τ is the number density of pores in the specimen, $(\rho_{\mathrm{matrix}} - \rho_{\mathrm{pores}})^2$ is the contrast factor between pores and matrix, V_{p} is the pore volume and $P(q)$ is the form factor of the pores.

Here we have considered the spherical form factor for $P(q)$. In reality for a ceramic system pores are not truly mono-disperse in size but a hierarchy of length scales exists.

For a polydisperse system the expression for scattered intensity can be expressed as

$$I(q) = C \int D(R) V_{\mathrm{p}}^2(R) P(q, R)\, \mathrm{d}R. \qquad (2)$$

In the present case it is assumed that polydisperse spherical pores are dispersed in the matrix. The distribution of sizes of the pores has been assumed to be lognormal in nature and the basis for this assumption is explained below.

A distribution of a variable is modeled as lognormal when the distribution is generated by many effects. Products of many small independent factors are responsible for the variation of the variable. A random variable X is said to be lognormally distributed if $\log(X)$ is normally distributed. The variable assumes only positive values and the distribution is skewed to the left. Skewed distributions are particularly common when mean values are low, variances are large and values of the variable cannot be negative, as in the present case for pore-size distribution in a ceramic. Skewed distributions often closely fit the lognormal distribution.

In a proportionate size-dependent growth process

$$r_{j+1} - r_j = k_j r_j$$

where r_j is the radius at the jth step of the growth process and k_j is a random number which varies between 0 and 1 depending upon factors responsible for growth.

For a natural growth process, there are many factors responsible for the size-dependent growth and, hence, the size distribution is often found to be lognormal [23b]. Such processes appear in various fields, such as environmental sciences, aerosol research, biology, medical sciences etc.

The prevailing operation in the laws of natural sciences is multiplication. For instance, the rate of a chemical reaction depends on the product of the concentrations of the molecules involved. Likewise, the coalescence probability of two different types of pores is determined by the product of their population densities. Equilibrium conditions are governed by factors that act in a multiplicative way and that is why the governing frequency distributions in nature usually favor the lognormal distribution.

Several independent factors are responsible for the formation of pores in ceramics. Hence, pore-size distribution has been modeled as a lognormal distribution. Further, a lognormal distribution could explain the present data well:

$$D(r, a, b) = \frac{1}{\sqrt{2\pi b^2 r^2}} \exp\left[-\frac{\left\{\ln\left(\frac{r}{a}\right)\right\}^2}{2b^2} \right]. \qquad (3)$$

It has already been mentioned (as evident from figure 2) that a shoulder-like feature exists in the scattering profiles for specimens with sintering temperatures beyond 1300 °C. It is also observed that this feature becomes more prominent with increasing sintering temperature. In other words, the shoulder-like feature is pronounced as porosity decreases. If looked at carefully, it is observed from figure 2 that the whole profile may be segmented into two zones, namely zone I (below $q = 0.15$ nm^{-1}) and zone II (above $q = 0.15$ nm^{-1}), respectively.

At this point it is interesting to discuss that the shoulder-like feature, as mentioned above, in SANS profiles cannot be quantified in terms of a peak as is evident from the nature of the derivative of the intensity with q (inset of figure 2). The derivative of the profiles has been shown in the inset of figure 2. It is clear from the inset that the derivative is not changing its sign near the shoulder-like feature. Hence, in the present case the above feature in the profile is termed as a 'shoulder'. The appearance of a shoulder in the scattering profile may originate from one of the following possibilities. Firstly, it may appear due to the correlation in the pore structure and manifests in the scattering profile. Secondly, the shouldering effect may be due to the modification in the pore-size distribution during sintering. Emergence of a bimodal pore-size distribution with well-separated modes during sintering is also a possibility. The first possibility, in the present case, can be discounted on the basis of the fact that the prominence of the shoulder-like feature increases with decreasing porosity. For the validity of the first possibility it should be the other way, i.e. the shoulder-like feature should be more pronounced when porosity is greater. So, the second possibility appears to be a more plausible reason in the present case.

For the specimen sintered at the temperature of 1300 °C, the shoulder does not exist and can be explained by a single pore-size distribution. Hence, the SANS profiles for specimens sintered beyond 1300 °C were analyzed by introducing a distribution function $D(r)$ which is the linear combination of the two distributions in order to explain the whole profile. Estimated pore-size distributions are depicted in figure 4. The number density of the larger size pores was found significantly smaller than that of the smaller size pores and hence the former distribution is not distinctly visible in figure 4 in linear scale. So, the larger pore-size distribution is plotted separately in the inset of the figure for clarity. It is interesting to note that, although the number density of the larger size pores is significantly smaller compared to that of the smaller size pores (ratio $\sim 10^{-4}$), the effect on the scattering profile is quite significant.

This is due to the fact that the scattering intensity depends on the sixth power of the radius (i.e. square of the volume) of the particles and the effect becomes significant as far

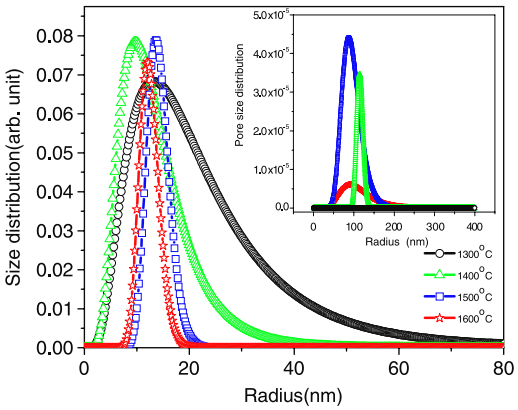

Figure 4. Combined pore-size distribution for different sintering temperatures. Inset shows separately the larger size distribution component only, which is otherwise not clearly visible in the main figure (see text).

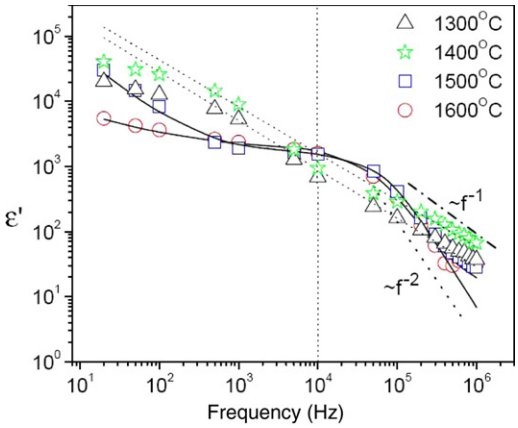

Figure 5. Real part (ε') of the dielectric response as a function of frequency for different sintering temperatures.

as the scattering intensity is concerned. As expected, the contribution from the larger size distribution modifies the profiles in zone I. The extracted parameters from the above model have been tabulated in table 1. From figure 4 and table 1, it has been observed that the average pore size is reduced and overall polydispersity of the pore-size distribution also decreased with increase in sintering temperature. It has also been observed from table 1 that, as expected, porosity decreases significantly as sintering temperature is increased and the pellets becomes denser. These observed variations in pore structure and porosity can be explained on the basis of the sintering theory. High surface area/surface energy of particles provides the driving force for sintering. Thus, coalescence of smaller particles into bigger particles occurs via a mass transport diffusion process during sintering. This leads to a reduction in surface area. Hence, this results in shrinkage of the matrix and decrease in porosity. Thus, the density of the material increases towards its theoretical density upon sintering [12]. Also, at higher sintering temperature grain size increases and the pores tend to break away from the grain boundaries and become spherical. Smaller pores are eliminated, while larger pores can grow.

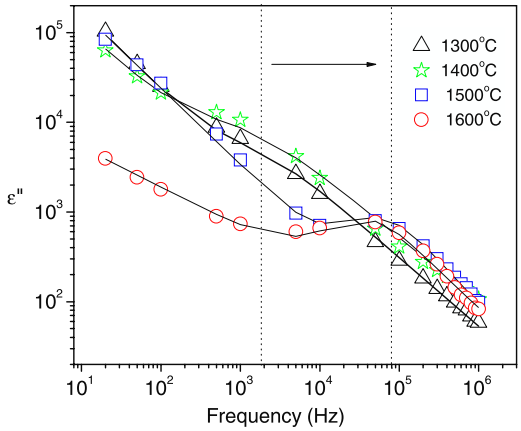

Figure 6. Imaginary part (ε'') of the dielectric response as a function of frequency for different sintering temperatures.

Emergence of the shoulder-like feature is basically due to the decrease in polydispersity of the combined pore-size distribution and the appearance of the second-larger length scale pore-size distribution with sintering temperature.

From figure 5 it is discernible that the frequency dependence of ε' shows a significant change above 10^4 Hz. For samples sintered up to 1400 °C, the high frequency variation of ε' shows f^{-1} dependence, i.e. the slope of the straight line in a double logarithmic plot is -1. However, the situation is significantly different for the samples sintered at higher temperatures. In this case the dependence of ε' at the higher frequency regime is $\sim f^{-2}$, yielding a slope of the straight line of the log–log plot of -2. So, there is a change of slope from -1 to -2 as the sintering temperature is increased.

Like the variation in the real part of the permittivity, the imaginary part is also significantly altered by sintering vis-á-vis the pore structure modification. From figure 6 it is evident that the imaginary part shows some kind of peak-like feature (at $f \sim 8\times10^4$ Hz) for the specimen sintered at 1500 and 1600 °C. A closer look at figure 6 shows a broadened peak/hump-like feature at around a frequency $\sim 2 \times 10^3$ Hz. However, it is seen that the anomalous increase near the low frequency region shadows the exact peak position. It means peak-like structures exist even in this case but they are not very pronounced as compared to profiles for pellets sintered at 1500 and 1600 °C. It is also interesting to observe that the dielectric loss increases as frequency decreases in the low frequency regime.

The dielectric loss peak is represented empirically by the Jonscher model [24], which is also known as the universal dielectric response (UDR) and can be expressed as

$$\varepsilon''(f) = \frac{c_3}{\left(\frac{f}{f_p}\right)^{-m} + \left(\frac{f}{f_p}\right)^{1-n}} \tag{4}$$

where f_p characterizes the peak frequency. Here exponents m and $1 - n$ both vary in the range 0–1. A Debye-type response corresponds to both these exponents being equal to unity, i.e. the situation with $m = 1$ and $n = 0$. When the exponents m and $(1 - n)$ are both close to unity then the response is called a near-Debye type. Then, when the m and

$(1-n)$ exponents are far from unity the response is called non-Debye. It is noteworthy that a classical Debye-type response corresponds to a non-interacting dipolar system. A non-Debye-type response corresponds to an interacting dipole system and the parameters m and $(1-n)$ represent the degree of correlation between dipoles.

However, equation (4) does not take into account the anomalous increase in the low frequency regime. This can be accounted for by a modification of equation (4) by adding a power law term in it [25]. Thus, to fit the whole spectrum, including the low frequency anomalous increase, the following expression was used:

$$\varepsilon''(f) = \frac{c_3}{\left(\frac{f}{f_p}\right)^{-m} + \left(\frac{f}{f_p}\right)^{1-n}} + c_4 f^{m_1}. \tag{5}$$

Thus, in equation (5) the first term corresponds to the dielectric response which involves a relaxation process, which occurs primarily in dipolar systems. The second term corresponds to the response from the charge carrier's movement such as conduction, hopping, jump, diffusion etc, which is mainly responsible for the loss in the dielectric materials at lower frequencies. So the dielectric response of the samples can be broadly divided into two parts: a low frequency contribution due to charge carrier transport and a high frequency contribution due to dipolar relaxation processes.

It is clear from the dielectric data (figure 6 and table 1) that for the pellets sintered at 1300 and 1400 °C the imaginary part of the dielectric response is best fitted for $m = 0.42$ and 0.39, and $n = 0.25$ and 0.28, respectively. As described earlier this situation, i.e. the strong deviation of m and $(1-n)$ from unity, correspond to a non-Debye-type response. In contrast, for the case of pellets sintered at 1500 and 1600 °C the imaginary part of the response is best fitted with $m = 1.0$ and 0.99, and $n = 0.005$ and 0, respectively. This situation corresponds to the near-Debye-type dielectric response. This indicates a transition of the dielectric response from non-Debye-type to near-Debye-type occurs with an increase in sintering temperature vis-á-vis modification of the pore structure and pore connectivity.

To confirm the above findings let us concentrate on the frequency dependence of the real part of the response. For the non-Debye-type response for $f > f_p$, the expression for ε' can be derived from equation (5) by Kramers–Kronig relations, where the real part of the permittivity at high frequency can be written as

$$\varepsilon'(f) = cf^{n-1} \tag{6}$$

with the same criteria on n as mentioned earlier. It is observed that, with the same values of n, the real part of the dielectric spectra fits quite well for both 1300 and 1400 °C sintering temperatures. Similarly, a near-Debye-type response has been observed from the imaginary part of the response for the pellets sintered at 1500 and 1600 °C. To confirm this a classical Debye-type response for the real part of the dielectric spectra $\varepsilon'(f) = \frac{c_1}{1+(\frac{f}{f_p})^2}$ has been adopted for $f > f_p$ for 1500 and 1600 °C samples.

Although the above equation fits quite well for $f > f_p$ due to an increasing trend at low frequency the whole frequency spectrum could be best fitted with an additional term in order to fit the frequency spectrum in the lower frequency regime:

$$\varepsilon'(f) = \frac{c_1}{1 + \left(\frac{f}{f_p}\right)^2} + c_4 f^{-k}. \tag{7}$$

The above model fits the real part of the response for 1500 and 1600 °C. Thus the above analysis for the real part of the permittivity further confirms the transition from a non-Debye-type to near-Debye-type dielectric response.

As mentioned earlier interfacial polarization across a pore boundary results in a dipolar system. The pore network at relatively lower sintering temperature (below 1400 °C) is expected to be somewhat random and polydisperse in nature. At this temperature pores are connected to some extent and porosity is larger and results in an interacting dipolar system. With increase in the sintering temperature, the pores become more isolated and less polydisperse. So, when the sintering temperature is below 1500 °C a non-Debye-type response appears and is primarily attributed to the interconnected polydisperse pores with rough pore–matrix interface. As mentioned earlier the SANS data corroborates these observations. When the sintering temperature is enhanced beyond 1400 °C, the overall polydispersity of the size distribution and also porosity decreases significantly. These modifications in pore structure may be attributed to the mass transport during sintering [12]. Also, the connectivity of pores breaks as sintering temperature is increased. Sintering at higher temperatures gives rise to a smoothening of the pore–matrix interface [31] while the interfaces remain rough at lower sintering temperatures.

Smoothening of pore walls and reduction in total surface area are realities in normal sintering processes but the reduction of porosity during sintering cannot induce a most probable separation distance between the pores. If at all, correlation between the pores will decrease with sintering as the population decreases. As the total volume of pores decreases with sintering, the increase in population of pores to induce the most probable separation more effectively will only result in increased interface area. This is certainly not the case here.

Thus, the aforementioned geometrical modifications in the pore structure upon sintering results in a non-interacting dipole system. This in turn leads to a near-Debye-type response.

From figure 6 and table 1 it has also been observed that the peak frequency of the dielectric loss for 1300 and 1400 °C sintering temperature does not alter significantly within the error bar. A similar trend is observed for 1500 and 1600 °C sintered samples but the peak frequency is significantly shifted towards the higher frequency side as sintering temperature is increased from 1400 to 1500 °C.

The peak frequency depends on the activation energy and can be written as $f_p \propto \exp(-\frac{W}{kT})$. In earlier studies on porosity dependence [26–30] of the dielectric response, it has been shown that the activation energy depends on specific pore surface area and porosity. As the sintering temperature is enhanced the specific surface area of the pores decreases, which results in shifts in the peak frequency towards the higher side.

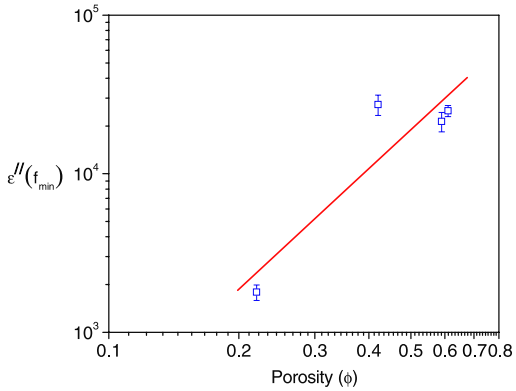

Figure 7. Variation of dielectric loss (ε'') at very low frequency with porosity of specimens.

It is also noteworthy to mention that loss at low frequency decreases significantly with sintering temperature. The variation of ε'' at the lowest available frequency (∼40 Hz) with porosity (at different sintering temperature) has been depicted in figure 7.

It can also be understood in terms of Archie's phenomenological law for real conductivity $\sigma'(0)$ (i.e. is proportional to the complex part of the permittivity $\varepsilon''(0)$) $\propto \phi^m$ where ϕ is the porosity of the medium. The exponent m is called the cementation index and it ranges experimentally between $m \sim 1$ and $m \sim 4$.

The cementation index has been found in the present case to be 2.52 ± 0.80.

4. Conclusions

Reduction in polydispersity of the pore-size distribution in nanocrystalline $YCrO_3$ occurs as the sintering temperature is enhanced. A shoulder-like feature in SANS data beyond a sintering temperature of 1400 °C is attributed to the significant modifications in the pore structure and emergence of bimodal pore-size distributions with well-separated modes upon sintering.

The dielectric response in the frequency range 0.2–100 kHz showed a strong dependence on the pore characteristics. A transition from non-Debye response to near-Debye response was observed as sintering temperature is increased beyond 1400 °C and is corroborated by the results obtained from the SANS analysis. This is attributed to the combined effect of pore–matrix interface smoothening, reduction of polydispersity of the pore-size distribution and breaking of the connectivity of the pores with increasing sintering temperature.

Acknowledgments

We would like to thank Drs S K Mishra and V K Aswal of the Solid State Physics Division, Bhabha Atomic Research Centre, Mumbai, India for their kind help in dielectric and SANS measurements, respectively.

References

[1] Bowen C R and Almond D P *Mater. Sci. Technol.* **22** 719
[2] Hippel Von 1954 *A R Dielectrics and Waves* (New York: Wiley)
[3] Wood V E and Austin A E 1975 *Magnetoelectric Interaction Phenomena in Crystals* ed A J Freeman and H Schmid (London: Gordon and Breach)
[4] Serrao C R, Kundu A K, Krupanidhi S B, Waghmare U V and Rao C N R 2005 *Phys. Rev.* B **72** 220101(R)
[5] Jonscher A K 1975 *Nature* **253** 717
[6] Niklasson G A 1987 *J. Appl. Phys.* **62** 258
[7] Penn S J, Alford N M, Templeton A, Wang X, Xu M, Reece M and Schrapel K 1997 *J. Am. Ceram. Soc.* **80** 1885
[8] Valant M and Suvorov D 2003 *Mater. Chem. Phys.* **79** 104
[9] Alford N M and Penn S J 1996 *J. Appl. Phys.* **80** 5895
[10] Maxwell J C 1954 *A Treatise on Electricity and Magnetism* vol 1 (New York: Dover)
[11] Wagner W 1914 *Arch. Elektrotech.* **2** 371
[12] Kingery W D, Bowden H K and Uhlmann D R 1976 *Introduction to Ceramics* (*Wiley Series on the Science and Technology of the Materials*) 2nd edn (New York: Wiley) p 1032
[13] Sen D, Patra A K, Mazumder S and Ramanathan S 2002 *J. Alloys Compounds* **340** 236
[14] Sen D, Patra A K, Mazumder S and Ramanathan S 2003 *J. Alloys Compounds* **361** 270
[15] Sen D, Mahata T, Patra A K, Mazumder S and Sharma B P 2003 *J. Alloys Compounds* **364** 304
[16] Sen D, Mazumder S and Tarafdar S 2002 *J. Mater. Sci.* **37** 941
[17] Patra A K, Bahadur J, Mazumder S, Sathi Nair, Purohit R D and Tyagi A K 2007 *J. Nanosci. Nanotechnol.* **8** 1
[18] Bedekar V, Shukla R and Tyagi A K 2007 *Nanotechnology* **18** 155706
[19a] Mazumder S, Sen D, Saravanan T and Vijayaraghavan P R 2001 *J. Neutron Res.* **9** 39
[19b] Aswal V K and Goyal P S 2000 *Curr. Sci.* **79** 947
[20] Mazumder S and Sequeira A 1992 *J. Appl. Crystallogr.* **25** 221
[21] Lake J A 1967 *J. Appl. Crystallogr.* **23** 191
[22] Mazumder S, Jayaswal B and Sequeira A 1998 *Physica* B **241–243** 1222
[23a] Mazumder S and Sequeira A 1990 *Phys. Rev.* B **41** 6272
[23b] Maul J, Marosits E, Sudek C, Berg T and Ott U 2005 *Phys. Rev.* B **72** 245401
[24] Jonscher A K 1983 *Dielectric Relaxation in Solids* (London: Chelsea)
[25] Jonscher A K, Meca F and Millany H M 1979 *J. Phys. C: Solid State Phys.* **12** L293
[26] Hilfer R 1992 *Phys. Scr.* T **44** 51
[27] Hearst J R and Nelson P H 1985 *Well Logging for Physical Properties* (New York: McGraw-Hill)
[28] Keller G V and Licastro P H 1959 *US Geol. Surv. Bull.* **10528** 257
[29] Keller G V 1982 *Handbook of Physical Properties of Rock* ed R A Carmichael (Boca Raton, FL: CRC Press) p 217
[30] Sen D, Mahata T, Patra A K, Mazumder S and Sharma B P 2004 *J. Phys.: Condens. Matter* **16** 6229
[31] Sen D, Bahadur J, Mazumder S, Bedekar V and Tyagi A K 2008 *J. Phys.: Condens. Matter* **20** 035103